Precursor Adsorption On Copper Surfaces As The First Step During The Deposition Of Copper: A Density Functional Study With Van Der Waals Correction

*Yasheng Maimaiti and Simon D. Elliott**

Tyndall National Institute, University College Cork, Lee Maltings, Prospect Row, Cork, Ireland

KEYWORDS: Atomic layer deposition, Copper thin film, Density functional theory, van der Waals interactions, Copper dimethylamino-2-propoxide.

ABSTRACT: Copper dimethylamino-2-propoxide [$Cu(dmap)_2$] is used as a precursor for low temperature atomic layer deposition (ALD) of copper thin films. Chemisorption of the precursor is the necessary first step of ALD, but it is not known in this case whether there is selectivity for adsorption sites, defects or islands on the substrate. Therefore we study the adsorption of the $Cu(dmap)_2$ molecule on the different sites on flat and rough Cu surfaces using PBE, PBE-D3, optB88-vdW and vdW-DF2 methods. We found the relative order of adsorption energies for $Cu(dmap)_2$ on Cu surfaces is E_{ads} (PBE-D3) > E_{ads} (optB88-vdW) > E_{ads} (vdW-DF2) > E_{ads} (PBE). The PBE and vdW-DF2 methods predict one chemisorption structure, while optB88-vdW predicts three chemisorption structures for $Cu(dmap)_2$ adsorption among four possible adsorption

configurations, whereas PBE-D3 predicts a chemisorbed structure for all the adsorption sites on Cu(111). All the methods with and without van der Waals corrections yield a chemisorbed molecule on the Cu(332) step and Cu(643) kink because of less steric hindrance on the vicinal surfaces. Strong distortion of the molecule and significant elongation of Cu – N bonds is predicted in the chemisorbed structures, indicating that the ligand – Cu bonds break during the ALD of Cu from $Cu(dmap)_2$. The molecule loses its initial square planar structure and gains linear O – Cu – O bonding as these atoms attach to the surface. As a result, the ligands become unstable and the precursor becomes more reactive to the co-reagent. Charge redistribution mainly occurs between the adsorbate O – Cu – O bond and the surface. Bader charge analysis shows that electrons are donated from the surface to the molecule in the chemisorbed structures, so that the Cu center in the molecule is partially reduced.

INTRODUCTION

Thin films of metals have a wide range of current and future applications in many technologies such as microelectronics,[1] plasmonic devices,[2] spintronics[3] and catalysis[4]. Atomic layer deposition (ALD) is one of the most promising techniques to deposit highly uniform and conformal thin films.[5] Metal thin films have been deposited both with thermal and plasma ALD using metalorganic compounds as precursors. In ALD, the first precursor adsorbs on the substrate in one ALD pulse and reacts at the surface with reducing co-reagents during the second pulse.[1,6] In contrast with the ALD of other metals, ALD growth of Cu has been relatively well established because of the availability of Cu precursors and because of the technological demand for Cu as a main interconnect material in electronics. Although several Cu ALD processes that use different Cu(I) and Cu(II) metalorganic compounds and co-reagents have been developed in the past,[7–10] a notable advance in low temperature Cu ALD processing was made by employing

the reaction of copper dimethylamino-2-propoxide [$Cu(dmap)_2$] with diethylzinc (Et_2Zn) at temperatures of 100 – 120 °C.[11] The growth mechanism of this process has been investigated using density functional theory (DFT) in a gas-phase model and it is predicted that the surface is probably covered with a Cu(I) intermediates.[12] Later, a thin film of very pure Cu has been deposited using a three-step ALD process which entails the sequential reactions of $Cu(dmap)_2$, formic acid and hydrazine (N_2H_4) at 120 °C.[6] Recently, low temperature Cu ALD has also been demonstrated using a two-step process of $Cu(dmap)_2$ and borane dimethylamine [$BH_3(NHMe_2)$] and a three-step process using $Cu(dmap)_2$, formic acid and $BH_3(NHMe_2)$.[13] In these cases, the $Cu(dmap)_2$ precursor is successful because of its relatively high vapor pressure and thermal stability. Given these promising developments, the reaction mechanism and surface chemistry of $Cu(dmap)_2$ precursor during Cu ALD should be carefully investigated in order to identify better precursors and design new ALD processes for Cu as well as other metals.

In particular, we are interested to find out whether there is selectivity in the adsorption of molecules like $Cu(dmap)_2$ onto a growing Cu surface, and whether growth at islands or edges is favoured over layer-by-layer growth of the smooth surface. Island growth is one of the obstacles towards the use of ALD in the semiconductor industry.[9] The first step in a typical ALD process is the chemisorption of the precursor molecule on the surface, which is followed by a series of surface reactions, some of which may be irreversible due to desorption of by-products. The subsequent reactions are not possible in the case of weaker physisorption because the physisorbed precursors tend to desorb first, meaning that no ALD takes place. Thus, it is imperative to carefully investigate the adsorption of the precursors on the substrate. Zaera *et al.* studied the adsorption of metal ALD precursors on a metallic substrate using temperature programmed desorption (TPD) and X-ray photoelectron spectroscopy and showed the usefulness

of experimental surface chemistry methods for the development of ALD.[14–16] Computational approaches such as electronic structure theory calculations can also be an efficient way to investigate the surface chemistry and reaction mechanism and thus shorten the process development time in the laboratory. However, very few computational studies on the surface chemistry of metal ALD are available in the literature.[17]

Accurate description of the interaction between organometallic precursors like $Cu(dmap)_2$ and the substrate poses a theoretical challenge because the origin of the precursor/substrate interaction is complex, resulting mainly from a balance between van der Waals (vdW) interactions, charge transfer, Pauli repulsion, covalent and ionocovalent bonds and interaction between the permanent dipole of the adsorbates and image dipoles in the substrate.[18] Of these, the vdW interaction is poorly described in standard DFT functionals. A large supercell is necessary to include the $Cu(dmap)_2$ adsorbate (39 atoms, 9 Å in diameter), which makes the system computationally expensive, and thus using a higher level method such as the random phase approximation is not feasible at present.[19] New approaches for the approximate treatment of vdW interactions at the DFT level have recently been implemented, and so we are interested to discover whether they make it possible to quantitatively describe the interaction of the organometallic precursor with the substrate.

In the present theoretical work, we study the adsorption of the $Cu(dmap)_2$ molecule on Cu surfaces using DFT with various levels of treatment of vdW forces. This work specifically aims (i) to study the energetic, geometric and electronic properties of adsorbed $Cu(dmap)_2$ on different adsorption sites on the Cu substrate (both flat and rough bare surfaces); (ii) to investigate the role of vdW interactions between the molecule and surface in the initial stage of Cu ALD using several vdW inclusive DFT schemes; and (iii) to discuss the implications of various adsorption

geometries of $Cu(dmap)_2$ for understanding the surface chemistry, island growth and reaction mechanism of ALD of copper.

THEORETICAL METHOD

Computational Details. The Vienna ab initio simulation package (VASP 5.3) was used for the periodic DFT calculations.[20] The projector augmented wave (PAW) approach[21] was applied for describing the effective potential of core electrons. The generalized gradient approximation (GGA) was employed with the exchange correlation functional of Perdew, Burke and Ernzerhof (PBE).[22] As Cu has a partially filled d shell, spin polarized calculations were performed throughout. Nevertheless, the resulting total spin moment was zero. The wave functions were expanded in the plane wave basis up to a cutoff energy of 450 eV. Because of the large cell sizes, it was found to be adequate to use only the Γ point to sample the Brillouin zone for both slab and gas phase calculations. The atomic positions of ions were optimized using a conjugate gradient algorithm until the forces on each ion were smaller than 0.02 eV/Å. The geometry optimization for a single $Cu(dmap)_2$ molecule in the gas phase was performed by placing the molecule in a rhombohedral supercell with $\gamma = 60°$ and a side length of 25 Å. The molecular orbital calculations were performed with the TURBOMOLE 6.4 suite of quantum chemical programs[23] using DFT within the GGA paramerization by PBE,[22] the resolution-of-identity (RI) approximation[24,25] and a split valence polarization basis set (def2-SVP).[26] The climbing-image nudged elastic band (CI-NEB) method was used for calculations of energy barriers between physisorbed and chemisorbed states.[27,28]

Treatment of VdW Interaction. Since no experimental data are currently available for the adsorption configuration of $Cu(dmap)_2$ on the Cu surface, it is not straightforward to fully

validate our calculations and assess the role of vdW interaction for this system. The vdW interactions are found to be crucial for computing reliable geometries and energies for various organic/inorganic interfaces.[19] Thus, we choose several vdW inclusive DFT methods along with pure PBE to assess the role of vdW interactions for the $Cu(dmap)_2$/Cu interface. Several articles give a detailed review of the development and challenges of vdW inclusive DFT methods.[19,29] The adsorption of a benzene molecule on metals is one of the most popular model systems to assess the performance of vdW inclusive DFT for the organic/solid interface.[30–35] Interatomic pairwise DFT-D methods by Grimme[36,37] are found to systematically overestimate the adsorption energies of benzene and several other molecules on metal surfaces.[35,38,39] As a result, they are used to represent an upper bound of the adsorption energy.[38,40] Hence, for this purpose we choose the latest version of this semi-empirical dispersion correction (PBE-D3)[37] with Becke-Johnson (BJ) rational damping.[41] The vdW-DF functional[42] and its second version (vdW-DF2)[43] are known to yield even smaller adsorption energies than PBE for various systems.[34,44–46] We therefore use the vdW-DF2 functional to estimate the lower bound of the adsorption energies. Yildirim *et al.* studied the adsorption characteristics of benzene on coinage and transition metals to compare the performance of different vdW functionals.[31] They found that optPBE-vdW and optB88-vdW[43] functionals show systematically good agreement with "averaged" experimental adsorption energies. A comparative study by Carrasco *et al.* on the performance of the two classes of vdW-inclusive methods (the PBE+vdW[47] and the PBE+vdW^{surf} methods[48]) for benzene adsorption on transition metals suggests that PBE+vdW^{surf} and optB88-vdW predict adsorption energies and equilibrium geometries that are in equally good agreement with experimental data.[34] Keeping these in mind, we also choose the optB88-vdW method which is

available in the VASP code. To conclude, the vdW inclusive methods that we have chosen in this paper along with pure PBE are PBE-D3, vdW-DF2 and optB88-vdW.

Adsorption Models. The calculated lattice parameters of fcc bulk Cu using the chosen vdW inclusive methods and PBE are 3.63 Å (PBE), 3.57 Å (PBE-D3) 3.74 Å (VDW-DF2) and 3.62 Å (optB88-vdW), compared with the experimental value of a_0=3.61 Å.[49] These lattice parameters are used to build corresponding slab models in each method. The slabs consist of four atomic layers of Cu. All atomic layers are allowed to relax within a fixed cell. A vacuum 18 Å thick was added so as to separate adjacent slabs with adsorbate.

During the ALD growth of copper, steps and kinks are likely to form on the surfaces with various geometries. Therefore three different Cu surfaces were used as substrates: flat Cu(111) surface, stepped Cu(332), and Cu(643) with a kink (see Figure 1). To accommodate the adsorbed precursor, a (6 × 6) surface expansion of Cu(111) is used, which gives the shortest H – H distance of 8.1 Å between adsorbate images in neighbouring cells and a precursor coverage of one $Cu(dmap)_2$ per 2 nm^2. As schematically illustrated in Figure 1a, we take four different adsorption configurations into account on the Cu(111) surface: these adsorption configurations are denoted as Cu(111)-T, Cu(111)-D, Cu(111)-M and Cu(111)-B according to the alignment of O – Cu – O bonds in the molecule relative to the surface. In the Cu(dmap)-T configuration, the adsorbate Cu atom aligns with the top of a Cu surface atom and the O atoms are slightly off the top of Cu atoms of one surface row. In Cu(111)-D, the O – Cu – O bond aligns with the long diagonal of four neighbouring Cu atoms. In this configuration, the two O atoms align on the top of two Cu surface atoms and the adsorbate Cu atom is at a bridge site. In the Cu(111)-M configuration, two O atoms are on the bridge sites and the adsorbate Cu atom is on the hollow site between rows. In the Cu(111)-B configuration, the adsorbate Cu atom is on a bridge site and

the O atoms are slightly off bridge sites of the same row. As we will show in the following sections, these adsorption configurations give completely different descriptions of $Cu(dmap)_2$ adsorption on the Cu(111) surface.

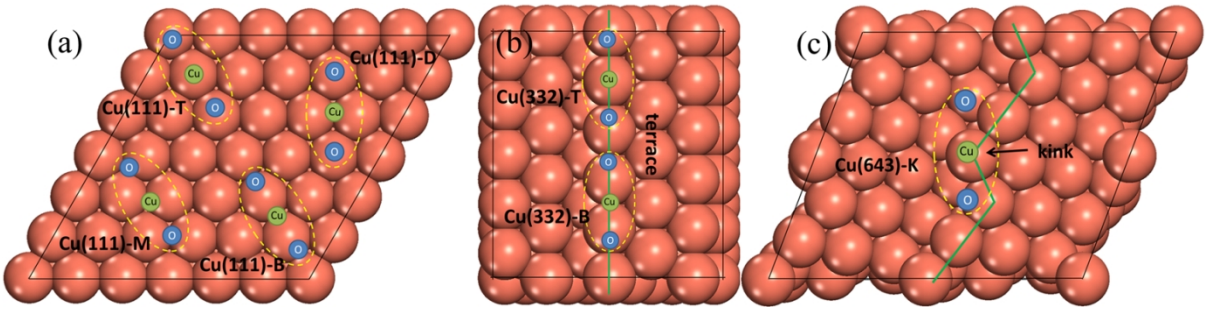

Figure 1. Adsorption models of $Cu(dmap)_2$ on different Cu surfaces. The initial position of O – Cu – O bonds of $Cu(dmap)_2$ on the surface are shown schematically. (a) Four adsorption sites on Cu(111) surface: Cu(111)-T, Cu(111)-D, Cu(111)-M and Cu(111)-B. (b) Two adsorption sites on the upper layer of the Cu(332) step: Cu(332)-T and Cu(332)-B. (c) Cu(643)-K. Abbreviations: T=top; D=diagonal; M=median; B=bridge; K=kink. The green lines on (b) and (c) show the edge atoms of the upper layer.

We use (5 × 1) and (2 × 2) surface expansions for the stepped Cu(332) surface and the Cu(643) surface with a kink, respectively (see Figure 1b-c). For the stepped Cu(332) surface, two different adsorption sites are considered: Cu(332)-T and Cu(332)-B. In the Cu(332)-T configuration, the adsorbate Cu atom is aligned on the top of a Cu atom on the edge and the O atoms is slightly off the top of Cu surface atoms on the same edge. In Cu(332)-T, the adsorbate Cu atom is at the bridge site between two Cu atoms on the edge, and the O atoms are slightly off the bridge sites of the same edge (Figure 1b). Only one configuration is considered for Cu(643)

because the kink only provides an adsorption site to the Cu atom in the molecule, and the ligands remain relatively distant (Figure 1c).

The adsorption energy, E_{ads}, is defined by

$$E_{\text{ads}} = -\left(E_{\text{precursor@surf}} - E_{\text{surf}} - E_{\text{precursor}}\right), \qquad (1)$$

where $E_{\text{precursor@surf}}$ and E_{surf} are the total energies of the slab with and without $Cu(dmap)_2$, respectively. $E_{\text{precursor}}$ is the total energy of the $Cu(dmap)_2$ molecule in the gas phase. A positive value of E_{ads} means that the adsorption is energetically favourable compared to isolated systems. All the calculated adsorption energies E_{ads} from PBE and vdW inclusive DFT are obtained starting from the same initial structure for each adsorption configuration as shown in Figure 1.

Examining the electronic charge density allows further analysis of the adsorption of $Cu(dmap)_2$ on different Cu surfaces. The charge density difference due to the adsorption of $Cu(dmap)_2$ on the surface is calculated as

$$\Delta\rho = \rho_{\text{precursor@surf}} - \left(\rho_{\text{surf}} + \rho_{\text{precursor}}\right), \qquad (2)$$

where $\rho_{\text{precursor@surf}}$ is the electronic charge density of $Cu(dmap)_2$ adsorbed on Cu surface, ρ_{surf} is the charge density of the relaxed Cu slab in the adsorption configuration without the presence of $Cu(dmap)_2$, and $\rho_{\text{precursor}}$ is the charge density of the molecule fixed in the adsorption geometry in vacuum. Bader charge analysis was performed to examine charge transfer between the molecule and the surface.[50] The theoretical scanning tunnelling microscopy (STM) images were visualized using the Hive software,[51] which implements the Tersoff-Hamann formalism.[52]

RESULTS

Below, we present the results of $Cu(dmap)_2$ adsorption on different adsorption sites on the flat and rough surfaces of Cu using DFT with different levels of vdW treatment. In the first section, we summarize and compare the energetics and adsorption geometries for the precursor adsorbed

on different adsorption sites. In the second section, through the charge density difference, we analyse how the electronic structure of the precursor/surface interface changes upon the adsorption.

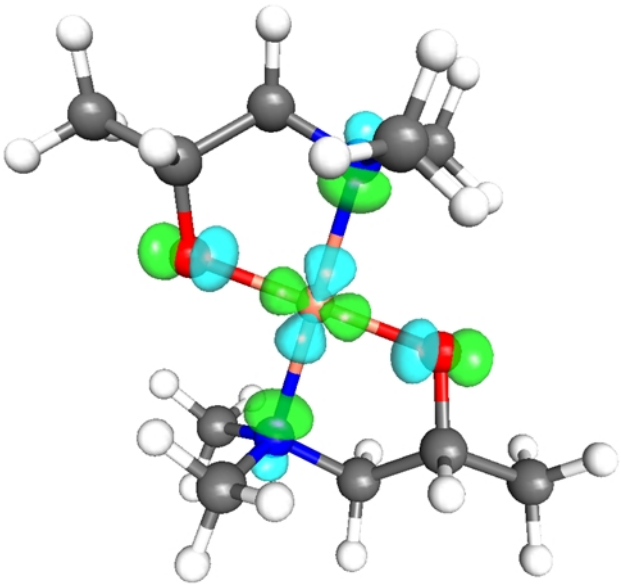

Figure 2**.** Optimized structure of copper dimethylamino-2-propoxide molecule [$Cu(dmap)_2$] with lowest unoccupied molecular orbital (LUMO). Colour scheme: red – O, blue – N, salmon pink – Cu, grey – C and white – H.

Adsorption Structure and Energy

Gas Phase $Cu(dmap)_2$. Figure 2 shows the optimized structure of the precursor molecule $Cu(dmap)_2$ with pure PBE. The $Cu(dmap)_2$ molecule contains two O and two N atoms, which coordinate to the central copper atom. The Cu atom forms two rings with the ligands, which are approximately co-planar, with angles of $\angle OCuO = 179.6°$ and $\angle NCuN = 178.3°$. The PBE computed Cu – O, Cu – N distances in $Cu(dmap)_2$ are 1.89 Å and 2.10 Å, respectively, in good agreement with experimental value of 1.87 Å and 2.07 Å.[53] The calculated geometric parameters from PBE-D3, optB88-vdW and vdW-DF2 are slightly different from those of PBE, as listed the Supporting Information (Table S1). Figure 2 also displays the lowest unoccupied molecular

orbital (LUMO), which is of Cu:d, O:p and N:p character, consistent with Cu^{2+} as the formal oxidation state, modified by the ionocovalent ligand – Cu bonding that is visible in the occupied orbitals (not shown). As examined below, the reactivity of the molecule mostly involves the interaction of Cu and O atoms with the surface, and the C, H, and N atoms of the dmap ligands are less reactive. The orientation of O – Cu – O bonding on the surface determines the how the molecule adsorbs (Figure 1).

Table 1. Adsorption energies (E_{ads}) and structural parameters of $Cu(dmap)_2$ adsorbed on different adsorption sites on bare Cu(111) surface including the adsorption height Z_{ad} (Å)[a], the distortion angle α (°)[b] and the Cu – N distance in the molecule $d_{Cu–N}$ (Å) obtained using PBE, PBE-D3, optB88-vdW and vdW-DF2 for different adsorption sites.

method	Properties	adsorption sites			
		Cu(111)-T	Cu(111)-D	Cu(111)-M	Cu(111)-B
PBE	E_{ads} (eV)	0.39	1.47	0.39	0.37
	Z_{ads} (Å)	3.96	2.27	4.02	4.12
	α (°)	8.3	39.7	7.6	5.1
	$d_{Cu–N}$ (Å)	2.05	2.55	2.04	2.04
	structure	**Figure 3**	**Figure 4**b	**Figure 3**	**Figure 3**
PBE-D3	E_{ads} (eV)	3.49	3.57	3.58	3.17
	Z_{ads} (Å)	2.40	2.22	2.24	2.22
	α (°)	36.1	36.7	37.5	35.6
	$d_{Cu–N}$ (Å)	2.34	2.33	2.40	2.27
	structure	**Figure 4**a	**Figure 4**b	**Figure 4**c	**Figure 4**d
optB88-vdW	E_{ads} (eV)	2.91	3.16	3.12	1.59
	Z_{ads} (Å)	2.41	2.23	2.18	3.69

	α (°)	38.8	38.6	39.6	8.3
	d_{Cu-N} (Å)	2.45	2.44	2.58	2.04
	structure	**Figure 4**a	**Figure 4**b	**Figure 4**c	**Figure 3**
vdW-DF2	E_{ads} (eV)	1.00	2.04	1.01	0.99
	Z_{ads} (Å)	3.88	2.30	3.93	3.98
	α (°)	9.9	39.5	8.8	4.3
	d_{Cu-N} (Å)	2.12	2.58	2.10	2.09
	structure	**Figure 3**	**Figure 4**b	**Figure 3**	**Figure 3**

[a]The adsorption height Z_{ads} is defined as the perpendicular distance between the adsorbate Cu atom and the surface Cu atoms averaged over the flat (111) surface or over the edge Cu atoms for the Cu(332) step. For Cu(643)-K, Z_{ads} is the distance between the adsorbate Cu atom and the outer kink atom on the Cu(643).

[b]The distortion angle α is defined as $\alpha = \frac{1}{2}(\angle\mathrm{NCuN(gas)} - \angle\mathrm{NCuN(adsorbed)})$, where $\angle\mathrm{NCuN(gas)}$ and $\angle\mathrm{NCuN(adsorbed)}$ are the N – Cu – N angles in gas phase and adsorbed $Cu(dmap)_2$, respectively.

Adsorption on Flat Surface. We investigate the adsorption of $Cu(dmap)_2$ on the Cu(111) surface for flat lying orientation. We choose four different adsorption sites, as shown in Figure 1a. **Table 1** displays the adsorption energies (E_{ads}) and selected geometric parameters including adsorption height Z_{ads}, distortion angle α and Cu – N bond distance d_{Cu-N} of each configuration. **Figure 3** and 4 show the different types of optimized geometries of $Cu(dmap)_2$ adsorption on these four sites on the Cu(111) using PBE, PBE-D3, optB88-vdW and vdW-DF2 methods.

As shown in **Table 1**, adsorption energies computed with PBE corresponding to Cu(111)-T, Cu(111)-M and Cu(111)-B vary slightly between 0.37 ~ 0.39 eV. The $Cu(dmap)_2$ molecule pushed away from the initial position on the surface after the optimization on these three adsorption sites, as shown in **Figure 3**. The distances between the adsorbate Cu atom and the surface (Z_{ads}) are around 3.9 – 4.1 Å. The distortion angle α is the change of the ∠NCuN angle after the adsorption and describes the degree of deformation of ligands around the Cu center. The

distortion angles α for these adsorption sites are between 5° and 8°. No chemical bonds are formed between the molecule and the surface and the gas phase structure of $Cu(dmap)_2$ is not significantly changed after the adsorption, which is indicative of physisorption.

Surprisingly, the adsorption energy computed from PBE is 1.47 eV for the Cu(111)-D, which is significantly greater than that computed for the other adsorption sites. This implies that the nature of the $Cu(dmap)_2$ adsorption is fundamentally different on the Cu(111)-D site. The optimized structure of $Cu(dmap)_2$ on Cu(111)-D (**Figure 4**b) shows that the molecule undergoes significant change relative to the gas phase in this configuration. The O atoms and Cu atom in the adsorbate bond to the surface Cu atoms and the adsorption height Z_{ads} is 2.27 Å. The bond lengths between adsorbate Cu and bonding surface Cu atoms are 2.62 Å, which is close to the computed Cu – Cu bulk distance (2.56 Å). The O atom – surface distances are 2.01 Å and close to the computed Cu – O distance in bulk CuO (1.95 Å).[54] The Cu – O distance in adsorbed $Cu(dmap)_2$ is 1.91 Å which is slightly bigger than the initial gas phase distance. The bond distances and adsorption energy at Cu(111)-D are thus characteristic of chemisorption. In order to release the stress between the molecule and the surface, the Cu – N distance has significantly elongated to become 0.44 Å longer than its gas phase distance. One CH_3 group on each N in the dmap ligands has changed its position to the upper side of the ligands. The distortion angle of $Cu(dmap)_2$ on the Cu(111)-D is around 40°, showing that the $Cu(dmap)_2$ molecule is strongly distorted and half-decomposed upon the adsorption.

We now describe the impact of vdW forces on $Cu(dmap)_2$ adsorption on the Cu(111) surface. As listed in **Table 1**, PBE-D3 produces adsorption energies of 3.1 – 3.6 eV for all the four adsorption configurations, which are considerably greater than those of pure PBE. In the Cu(111)-T configuration (**Figure 4**a), the O – Cu – O motif of the adsorbate forms bonds with

three adjacent Cu surface atoms in a row. The Cu surface atom under the adsorbate Cu atom is pushed slightly downward by 0.2 Å, while the Cu atoms that form bonds with the O atoms move slightly upward by 0.1 Å. The adsorption structure of $Cu(dmap)_2$ on Cu(111)-D obtained from PBE-D3 is similar to the structure found by pure PBE, which is shown in **Figure 4**b. The Cu(111)-M configuration (**Figure 4**c) yields a similar structure to Cu(111)-D, but the O atoms form bonds with Cu surface atoms in two neighbouring rows. In the Cu(111)-B configuration as shown in **Figure 4**d, the Cu and O atoms in the adsorbate each locate on the bridge site of the three consecutive surface Cu atoms with the Cu – Cu bond length of 2.56 Å and the O – Cu bond length of 2.06 Å. Notice the formation of triangular Cu_3 with the distance of 2.56–2.62 Å in all configurations. The adsorbate O atoms bond with the surface Cu atoms with the distance of 2.06 Å. For all the adsorption configurations on Cu(111) from PBE-D3, the adsorption height Z_{ads} varies between 2.2 and 2.4 Å and the distortion angle α is 36° – 38°. The Cu – N distance (d_{Cu-N}) in the adsorbate is stretched by 0.16 – 0.30 Å compared to the gas phase Cu – N distance. These results show that PBE-D3 describes the $Cu(dmap)_2$ adsorption on Cu(111) surface as strong chemisorption regardless of the adsorption site.

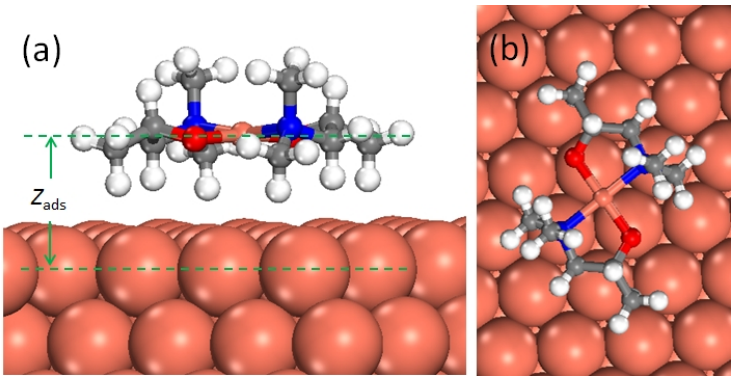

Figure 3. Physisorption structure of $Cu(dmap)_2$ on Cu(111) surface. (a) side view (b) top view.

As listed in **Table 1**, using optB88-vdW yields the adsorption energies E_{ads} in the range of 2.9–3.1 eV for Cu(111)-T, Cu(111)-D, Cu(111)-M configurations, which are lower than those calculated from PBE-D3, but higher than those from pure PBE. The optimized structures of Cu(111)-T, Cu(111)-D and Cu(111)-M configurations using optB88-vdW are represented in **Figure 4**a–c, respectively. The adsorption heights Z_{ads} are in the range of 2.2 – 2.4 Å, the distortion angle α varies between 38°– 39° and the Cu – N distance (d_{Cu-N}) is 0.2 – 0.4 longer than its gas phase distance. Thus Cu(111)-T, Cu(111)-D and Cu(111)-M configurations calculated with optB-vdW represent chemisorption. By contrast, the Cu(111)-B configuration has much lower adsorption energy of 1.59 eV with the same functional. Although this energy is higher than the adsorption energy which is calculated using pure PBE for the Cu(111)-D configuration, no chemical bonds are formed between the adsorbate and the surface. The adsorption height of 3.69 Å and the distortion angle of 8.3° implies that optB88-vdW predicts a physisorbed structure for Cu(111)-B, but with vdW interactions contributing an extra 1.2 eV to E_{ads} relative to PBE.

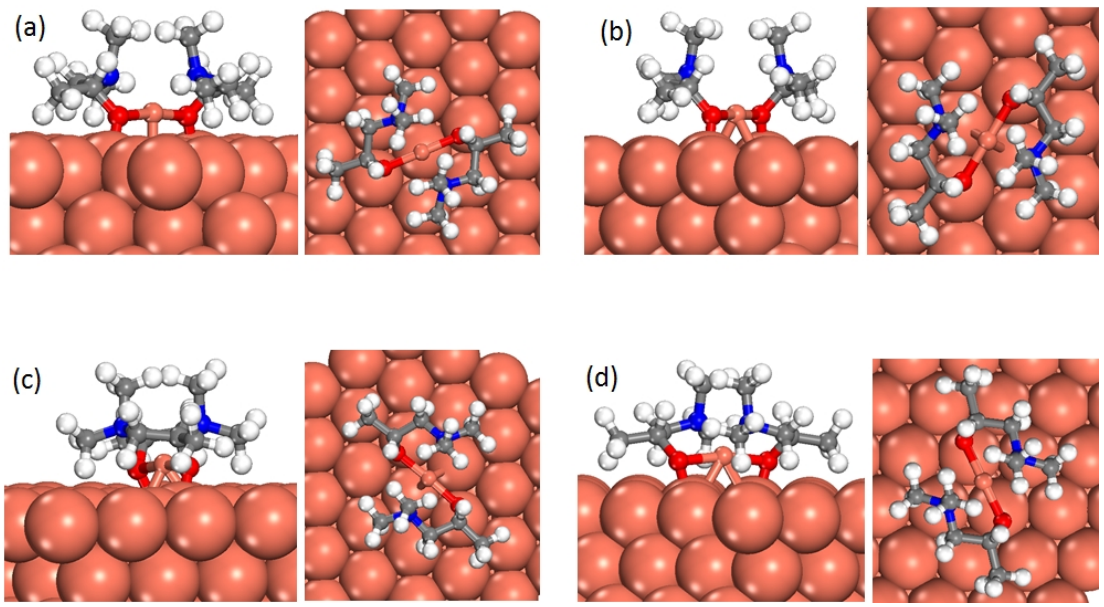

Figure 4. Side and top views of different adsorption structures of the $Cu(dmap)_2$ on the Cu(111) surface using DFT with and without vdW corrections (**Table 1**). (a) Cu(111)-T. (b) Cu(111)-B (c) Cu(111)-M (d) Cu(111)-B. Only the top two Cu layers of the slab are shown for clarity.

The calculations with the vdW-DF2 functional show E_{ads} of 2.04 eV for Cu(111)-D, which is twice as great as E_{ads} of Cu(111)-T, Cu(111)-M and Cu(111)-B (**Table 1**). The optimized structures for Cu(111)-D predicted with vdW-DF2 functional are shown in **Figure 4**b. The Cu – N distances have elongated to 2.58 Å and the distortion angle α is 39.5°. The vdW-DF2 functional thus predicts an additional 0.6 eV contribution from vdW attraction to the physisorption energy relative to pure PBE. The optimized structures of Cu(111)-T, Cu(111)-M and Cu(111)-B are represented in **Figure 3**. No chemical bonds are formed as the adsorption heights (Z_{ads}) are 3.9-4.0 Å and the distortion angles are small (4° – 10°) for these configurations. These data indicate that the adsorption mode of these structures is physisorption. It can be noticed that the PBE and vdW-DF2 both predict a chemisorbed structure on Cu(111)-D and

physisorbed structures at the other three adsorption sites, although the adsorption heights of the latter are slightly shorter than those predicted with pure PBE.

The above results show that two types of adsorption mode, namely physisorption and chemisorption, exist for $Cu(dmap)_2$ on the Cu(111) surface depending on the adsorption sites and the treatment of vdW interaction. It is interesting to ask whether these adsorption modes can interconvert. We therefore investigate the transition between physisorbed and chemisorbed states and assess the potential-energy surface (PES) by performing CI-NEB calculations.[27,28] **Figure 5** shows the pure PBE energy as a function of reaction coordinate, which is the collective change in the coordination of all the atoms in the molecule. We see that the PES is very flat near the physisorbed geometry and the transition from Cu(111)-T to Cu(111)-D proceeds with a small energy barrier (E_a = 0.17 eV for PBE), which is likely to be overcome at ALD temperatures, *e.g.* 100°C. As the vdW-DF2 functional also predicts a physisorbed structure on the Cu(111)-T site, we calculated the PES for the transition from Cu(111)-T to Cu(111)-D using the vdW-DF2 functional. We found that the vdW-DF2 method predicts that no appreciable energy barrier exists for the transition from physisorption (T) to chemisorption (D). However, here too the PES is very flat around the physisorption structure, so that such structures may exist for short lifetimes. Note that no minimum is obtained for physisorption using PBE-D3 and optB88-vdW.

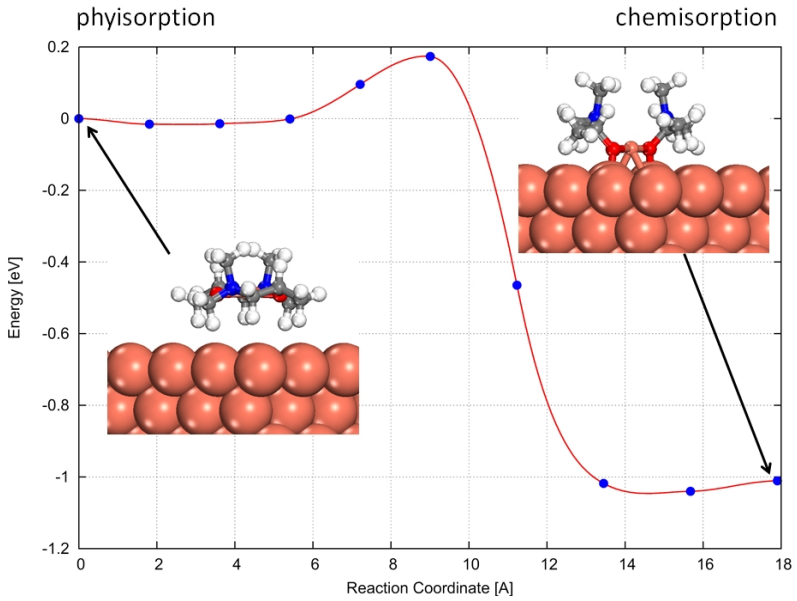

Figure 5. PBE reaction energy profile of transformation of $Cu(dmap)_2$ from physisorption at Cu(111)-T to chemisorption at Cu(111)-D.

Adsorption on rough surfaces. Steps and kinks are considered to be more reactive compared to flat surfaces like Cu(111) because of the under-coordinated edge and corner atoms.[55] We therefore calculate the adsorption of $Cu(dmap)_2$ on steps and kinks so as to understand the role of rough surfaces during ALD of copper. The Cu(332) step and the Cu(643) kink are chosen as the models for a rough surface in this study because they are the common steps and kinks that can be observed experimentally.[56,57] The optimized structures of adsorption on Cu(332)-T and Cu(643) are the structures from PBE calculations in **Figure 6**c-d, respectively. The adsorption energies and selected geometric parameters of those structures are displayed in **Table 2**. For the Cu(332)-B configuration, PBE, optB88 and vdW-DF2 yield a structure with adsorbate Cu – N bond elongation as shown in **Figure 6**a, while PBE-D3 predicts a structure with adsorbate Cu – O distance elongated as shown in **Figure 6**b. For Cu(332)-T and Cu(643)-K configurations, all the methods with and without vdW interactions produce similar structure.

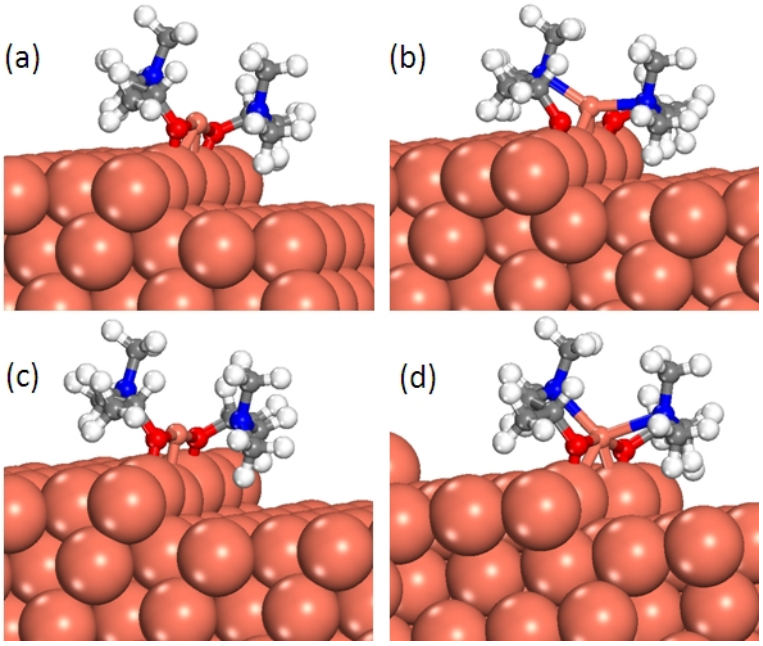

Figure 6. Adsorption geometry of $Cu(dmap)_2$ on rough Cu surfaces. (a) Cu(332)-B configuration obtained from PBE, optB86-vdW and vdW-DF2. (b) Cu(111)-B configuration obtained from PBE-D3. (c) Cu(332)-T and (d) Cu(643)-K from all the calculations.

PBE predicts an adsorption energy of 1.50 eV for the Cu(332)-B, which is slightly less than that of Cu(332)-T. In both structures (**Figure 6** 6a and c), the adsorbate O – Cu – O atoms in the $Cu(dmap)_2$ molecule form bonds with the three adjacent Cu atoms on the edge Cu atoms of the Cu(332) step. The adsorption height Z_{ads} is 2.2 Å for Cu(332)-B and 2.3 Å for Cu(332)-T. The distortion angles on Cu(332) steps are smaller than those of chemisorbed structures on Cu(111) surface by 5° – 10°. These smaller distortion angles indicate that the molecule is less distorted at the Cu(332) steps because of the less steric hindrance between the terraces and the molecule. The bond length between adsorbate O atoms and the surface Cu atoms are around 1.99 Å ~ 2.01 Å and the bonding Cu edge atoms shift slightly upward by 0.2-0.3 Å relative to the clean Cu(332) step. The ligands move toward the terraces and the Cu – N bonds elongate slightly to 2.27 Å.

Table 2. Adsorption energies (E_{ads}) and structural parameters of $Cu(dmap)_2$ adsorbed on rough Cu surfaces including the adsorption height Z_{ad} (Å), the distortion angle α (°) of $Cu(dmap)_2$ on the Cu surfaces and the Cu – N distance in the molecule $d_{Cu–N}$ (Å) obtained using PBE, PBE-D3, optB88-vdW and vdW-DF2.

method	Property	adsorption sites		
		Cu(332)-B	Cu(332)-T	Cu(643)-K
PBE	E_{ads} (eV)	1.50	1.53	1.78
	Z_{ads} (Å)	2.22	2.39	2.45
	α (°)	28.8	26.3	32.6
	$d_{Cu–N}$ (Å)	2.26	2.40	2.36
PBE-D3	E_{ads} (eV)	3.63	3.44	3.59
	Z_{ads} (Å)	2.09	2.37	2.40
	α (°)	19.3	22.1	29.3
	$d_{Cu–N}$ (Å)	2.01	2.17	2.26
optB88-vdW	E_{ads} (eV)	2.99	3.12	3.29
	Z_{ads} (Å)	2.25	2.36	2.31
	α (°)	26.5	27.1	31.4
	$d_{Cu–N}$ (Å)	2.20	2.23	2.32
VDW-DF2	E_{ads} (eV)	2.06	2.34	2.15
	Z_{ads} (Å)	2.26	2.43	2.48
	α (°)	27.4	29.9	32.2
	$d_{Cu–N}$ (Å)	2.33	2.38	2.75

PBE-D3 calculations predict an adsorption energy of 3.6 eV for Cu(332)-B and 3.4 eV for Cu(332)-B. For the Cu(332)-B adsorption site, PBE-D3 predicts a structure with significant

elongation of the adsorbate Cu – O bond, as shown in **Figure 6**b. The angle α is 19°. Unlike the other structures, the Cu – N bond length has shortened by 0.1 Å from its gas phase distance and the Cu – O bonds in the adsorbate have increased significantly by 0.9 Å, with these O atoms bonding to edge Cu atoms. However, for the Cu(332)-T configuration, PBE-D3 gives a structure with Cu – N bond elongation, which is similar to the Cu(332)-T structure predicted by the other methods.

We obtained E_{ads} of 3.0 eV and 2.0 eV at the Cu(332)-B step site using optB88-vdW and vdW-DF2 functionals, respectively. The optimized structures of Cu(332)-B with optB88-vdW and vdW-DF2 are again similar to the one predicted by PBE (**Figure 6**a), but with different adsorption heights and distortion angles as listed in **Table 2**. The Cu edge atom that bonds with the Cu atom in $Cu(dmap)_2$ is pushed downward by 0.2 – 0.4 Å and the Cu edge atoms that form Cu – O bonds are slightly pulled upward. The distortion angles α for these structures vary between 22° and 30°, smaller than those of the configurations on the Cu(111) surface because of less steric hindrance on the vicinal surfaces. Adsorption energies obtained with optB88-vdW and vdW-DF2 for the Cu(332)-T configuration are slightly greater than that of Cu(332)-B with these methods. The adsorbate O-Cu-O atoms bond to three adjacent edge atoms with the adsorption height of 2.3-2.4 Å and distortion angle of between 22° and 30°.

In the Cu(643)-K structure, the molecule is initially located on the outer kink atom on the Cu(643) surface at an initial Cu – O distance greater than 3 Å before optimization. All the methods with and without vdW correction produce a similar optimized structure for Cu(643)-K, and thus we only show the structure from PBE calculation in **Figure 6**d. As listed in **Table 2**, the calculated E_{ads} are 1.8 eV (PBE), 2.2 eV (vdW-DF2), 3.3 eV (optB88-vdW) and 3.6 eV (PBE-D3). In this structure, the adsorption height ranges from 2.4 to 2.5 Å, depending on the

functional, which is close to the Cu - Cu bulk distance. One of the O atoms bonds with the inner Cu kink atom and the other O atom bonds with the edge Cu atom neighbouring the outer kink Cu atom. The distortion angle ranges 29° ~ 33°, and the Cu – N distance $d_{Cu\text{-}N}$ varies between 2.3 and 2.6 Å. It is noteworthy that the outer Cu kink atom is significantly displaced (0.4 Å) from its bulk position in the vdW-DF2 calculations.

Electronic Structure

To further examine the interaction of $Cu(dmap)_2$ with the Cu surfaces, we analyse the electronic structure via the charge density difference (Equation 2), Bader charge and simulated STM images. We found that the 3D charge density difference plots and simulated STM images from DFT with and without additional vdW interactions are very similar for any given structure and we therefore only show the results for the Cu(111)-D, Cu(332)-T and Cu(643)-K configurations calculated with PBE.

The yellow and cyan regions in **Figure 7** represent the electronic charge accumulations and depletions respectively between the molecule and the surface. It can be observed that the charge accumulation and depletion are mainly confined to the area between the adsorbate O – Cu – O bonds and the surface. The electron accumulation (yellow) is mainly located on the bonds between the adsorbate and surface, while the electron depletion (cyan) is located on top of the O – Cu – O atoms and the two Cu surface atoms that attached to the O atoms. However, there is little change in the charge on C and H atoms in the ligands. This indicates that the interaction between $Cu(dmap)_2$ and the Cu surface is well localized and that the adsorption of the molecule mainly involves charge redistribution between the Cu and O atoms in the molecule and the surface. All the yellow regions are located on the molecule, indicating that the molecule gains electrons upon adsorption. The accumulation of electrons between the O atoms and the Cu

surface atoms suggest that covalent bonds are formed between the O atoms and the Cu surface. The large buildup of electrons around the bonds between the adsorbate Cu and the two Cu surface atoms is indicative of metallic bonding. This Cu_3 trimer shows a Cu-Cu(adsorbate)-Cu angle of 60.3° in the Cu(111)-D configuration. Yellow regions on the front and back of the N atoms can be observed, which indicates restoration of the N lone pair. The cyan regions and lack of yellow regions on the surface indicate that the surface donates electrons to the molecule from those surface Cu atoms that bond to the adsorbate O – Cu – O atoms.

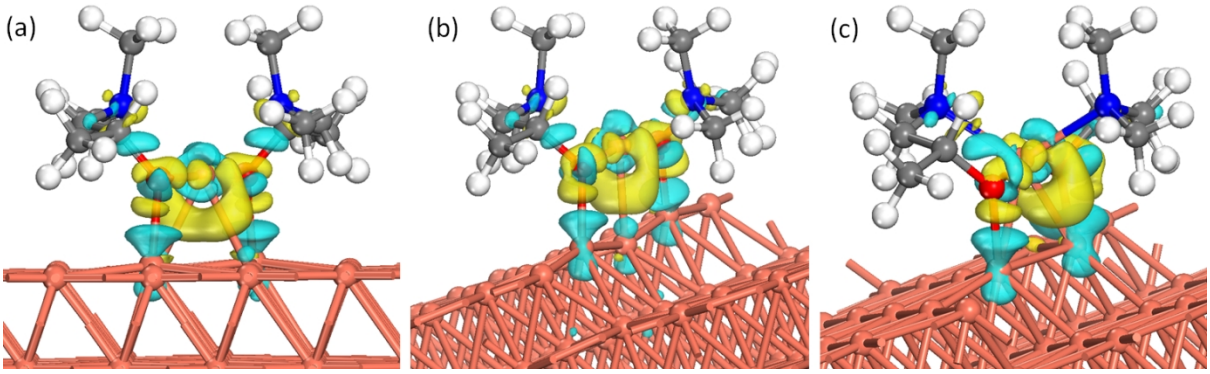

Figure 7. 3D isosurface of charge density differences obtained with an isovalue of ±0.001 e/Å^3 of $Cu(dmap)_2$ on (a) Cu(111)-D (b) Cu(332)-B (c) Cu(643)-K obtained using PBE. Yellow and cyan regions represent the accumulation and depletion of electronic charge, respectively.

In order to quantitatively analyse the charge redistribution, we calculated the net Bader charges on the adsorbate Cu atom (Δq_{Cu}) and on the molecule (ΔQ) relative to the Bader charge of the gas phase $Cu(dmap)_2$ molecule, as listed in **Table 3**. From **Table 3**, we can see that all the methods with and without additional vdW interaction produce the same order of Δq_{Cu} and ΔQ for a given structure. This indicates that the vdW interaction has little direct effect on the electronic structures of the adsorbed $Cu(dmap)_2$ molecule on Cu surfaces. The adsorbate Cu atom gains negligible electrons ($\Delta q_{Cu} < 0.1$ e$^-$) in all the physisorption structures and gains 0.2 ~ 0.4 e$^-$ in the

chemisorption structures depending on the adsorption sites and calculation method. The Bader charge analysis of the physisorbed structures reveals that a fraction of an electron is transferred from the molecule to the slab, where it is highly delocalised. By comparing the net charge differences for the various structures, we notice that the molecule gains electrons in all the chemisorbed structures. ΔQ of the whole molecule in the Cu(111)-D structure is slightly greater than ΔQ for other adsorption sites on the Cu(111) surface, which is in line with the stronger adsorption of Cu(111)-D. The electron gain of the molecule in the chemisorbed structure is consistent with what was observed in electron density difference plots (**Figure 7**) and probably originates from electron transfer to the LUMO (Figure 2). Notice that Δq_{Cu} and ΔQ of the Cu(332)-B structure predicted by PBE-D3 is significantly greater than those of other structures because of the breaking of the Cu – O bonds.

Table 3. Calculated change in Bader electronic charge (units of e^-) of adsorbate Cu atom (Δq_{Cu}) and $Cu(dmap)_2$ molecule (ΔQ) upon the adsorption of $Cu(dmap)_2$ on Cu surfaces relative to the Bader charge of the gas phase molecule.

	PBE		PBE-D3		optB88-vdw		VDW-DF2	
	Δq_{Cu}	ΔQ	Δq_{Cu}	ΔQ	Δq_{Cu}	ΔQ	Δq_{Cu}	ΔQ
Cu(111)-T	-0.08	-0.28	0.21	0.30	0.20	0.32	-0.02	-0.20
Cu(111)-D	0.25	0.34	0.23	0.31	0.24	0.32	0.26	0.39
Cu(111)-M	-0.07	-0.29	0.26	0.36	0.23	0.35	-0.04	-0.18
Cu(111)-B	-0.07	-0.31	0.23	0.31	-0.06	-0.29	-0.03	-0.18
Cu(332)-B	0.22	0.32	0.45	0.58	0.22	0.34	0.23	0.36
Cu(332)-T	0.20	0.33	0.18	0.28	0.19	0.32	0.23	0.39
Cu(643)-K	0.22	0.31	0.26	0.36	0.22	0.34	0.24	0.37

The methods we used in this work produce a range of adsorption energies and different adsorption structures. No experimental data exist at present against which the calculations can be validated in order to determine the best method. We therefore simulate theoretical STM images of the chemisorbed structures as a route towards validation in future experimental work. **Figure 8** depicts the simulated STM images of Cu(111)-D, Cu(332)-B and Cu(643)-K configurations calculated with PBE. In these STM images, the adsorbate Cu and O atoms are located in the darker part, which indicates that Cu and O atoms are close to the surface and far from the STM tip. We showed the atomic positions of adsorbate Cu (green) and O (red) in the right half of the STM images. The brightest regions of the STM images of the Cu(111)-D structure correspond to the methyl groups in the ligand, which face upward. Since the two ligands of the molecule are inclined at the rough surfaces, the brightness of upper parts of the STM images of Cu(332)-B and Cu(643)-K differ slightly.

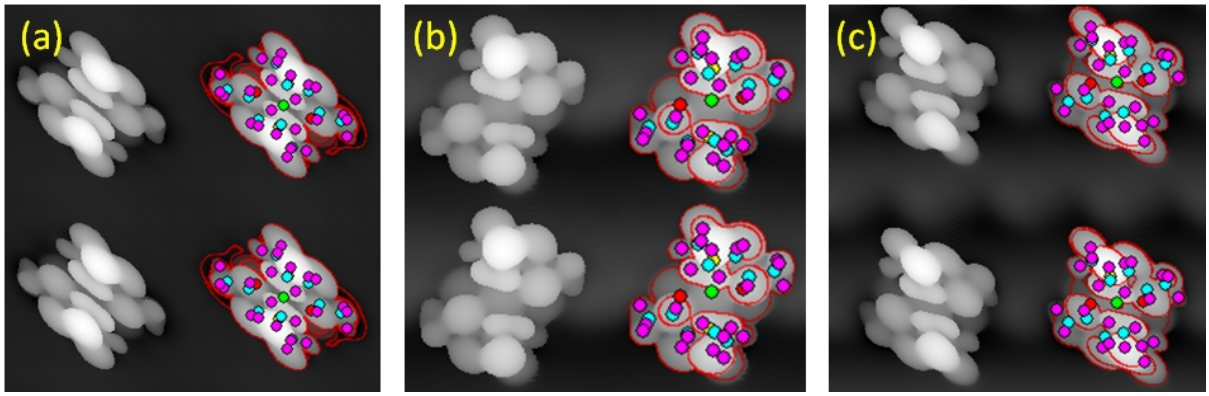

Figure 8. Simulated STM images of $Cu(dmap)_2$ adsorbed on (a) Cu(111)-D (b) Cu(332)-B (c) Cu(643)-K with bias voltage V = 1.5 eV and tip distance d = 1.5 Å. Contours are added on the right to guide the eye. The circles inside the contours show the positions of atoms in $Cu(dmap)_2$: green, Cu; yellow, N; red, O; aqua, C; pink, H.

DISCUSSION

Now we discuss the results of the $Cu(dmap)_2$ adsorption on different adsorption sites. First we analyse the geometric and electronic features of physisorption and chemisorption structures obtained by DFT with different levels of vdW treatment. Then we compare and assess the performance of these vdW treatments. Finally we discuss how the Cu atom in the $Cu(dmap)_2$ molecule is reduced during adsorption and the implications for Cu ALD processes.

Physisorption vs. chemisorption structure. The results show that the $Cu(dmap)_2$ molecule chemisorbs or physisorbs depending on the stereoselective environment on the Cu(111) surface. From the adsorption energy and structural changes in $Cu(dmap)_2$ calculated with PBE, we can see that $Cu(dmap)_2$ chemisorbs on the Cu(111)-D site and physisorbs on the other sites including Cu(111)-T, Cu(111)-M and Cu(111)-B. In order to explain this site-selective chemisorption on Cu(111)-D, one needs to look at its adsorption structure. The Cu(111)-D configuration allows the molecule to approach the surface with the shortest O–surface distance and with less steric hindrance between the ligands and the surface, which is not the case in the other structures. From the charge density difference plot, we can see that the strong ionocovalent bonds between O and surface Cu atoms hold the molecule attached to the surface and apparently overcome the Pauli repulsion forces and energetic cost of breaking Cu–N bonds. However, on the other three configurations on Cu(111), Cu–N bonds are not broken and Cu–O bonds are not formed because the O-surface distance is not short enough in the starting configurations. For the rough surfaces, it is predicted that the molecule chemisorbed onto the Cu(332) step and Cu(643) kink in all our calculations.

The geometric features of physisorbed $Cu(dmap)_2$ (**Figure 3**) include the long adsorbate-surface distance (approximately 4.0 Å) and the small distortion angle ($\alpha < 9°$). The molecule

undergoes only slight distortion and the Cu atom keeps its position in the planar coordination. Physisorption is characterized by a smaller adsorption energy (E_{ads} = 0.4 eV) for PBE, but of the order of 1.0 eV for the vdW-DF2 calculation.

On the other hand, chemisorption involves relatively high adsorption energy both with and without additional vdW interactions in DFT. These high adsorption energies are the net result of bond formation between the adsorbate O – Cu – O motif and the surface Cu atoms tempered by distortion. The new bonding causes an accumulation of stress between the precursor and surface that is generally released in the form of Cu – N breaking and the distortion of the rest of the ligands. The distortion of $Cu(dmap)_2$ can be characterized in the following ways. (i) The adsorbate Cu atom loses its position in the planar structure and obtains a linear structure in the O – Cu – O motif bonded with the surface. (ii) The Cu – N distances are elongated significantly by 0.2 to 0.5 Å (except for the Cu(332)-B structure with PBE-D3), but N remains oriented towards the Cu center. (iii) The Cu adsorption height Z_{ads} is comparable to the Cu – Cu bulk distance and the accumulation of charge between multiple Cu atoms is consistent with metallic bonding. (iv) The distortion angle α is greater than 26° (flat surface) and 19° (rough surface) and correlated with the Cu – N distance. The chemisorbed $Cu(dmap)_2$ molecule accepts electron density from the surface and the charge transfer mainly occurs in the region between adsorbate O – Cu – O bonds and the surface.

The impact of different levels of vdW treatment. The calculations with different levels of vdW treatment give different adsorption energies and optimized structures. Pure PBE predicts that $Cu(dmap)_2$ chemisorbs on Cu(111)-D and physisorbs on Cu(111)-T, Cu(111)-B, Cu(111)-M. The vdW-DF2 functional also predicts chemisorption at Cu(111)-D and physisorption at Cu(111)-T, Cu(111)-B and Cu(111)-M, but with E_{ads} nearly 0.6 eV greater. PBE–D3 predicts

chemisorption for all configurations, with the higher adsorption energies that are 2 eV greater than those obtained from pure PBE. The optB88-vdW method yields chemisorption on the three sites Cu(111)-T, Cu(111)-B and Cu(111)-M sites and physisorption on Cu(111)-B. This indicates that the vdW interactions act not only to increase the adsorption energies, but also to fundamentally change the nature of the adsorption.

It is reported that semi-empirical dispersion corrections (PBE-D) overestimate the adsorption energies for other organic/metal interactions.[58] This overestimation comes from the neglect of screening of dispersive interactions by the subsurface copper atoms. The adsorption energies of 3.2-3.5 eV predicted here by PBE-D3 are therefore most probably overestimated and thus represent the maximum limit. Although optB88-vdW predicts chemisorbed structures on three out of four configurations, the optB88-vdW energies for chemisorption are smaller than those of PBE-D3. The adsorption energy of chemisorbed Cu(111)-D from vdW-DF2 is less than that of PBE-D3 and optB88-vdW by 2.0 eV. The relative order of adsorption energies for $Cu(dmap)_2$ on Cu surfaces is E_{ads}(PBE-D3) > E_{ads}(optB88-vdW) > E_{ads}(vdW-DF2) > E_{ads}(PBE). This is the same order as was obtained for benzene/metal interations.[34,38] The difference between adsorption energy on rough surfaces are less dramatic, but they are in the same order as those of Cu(111). Thus we believe that optB88-vdW is the most suitable one of these methods for describing $Cu(dmap)_2$ adsorption on the Cu surfaces.

Our results from the charge density difference and Bader charge analysis show that the choice of vdW inclusive method has no significant impact on the electronic structure of the $Cu(dmap)_2$ adsorbate on Cu surfaces. For chemisorbed $Cu(dmap)_2$ on a certain adsorption site, all the methods predict similar electronic structures. Experimental STM study of $Cu(dmap)_2$ adsorption on the Cu surface could complement this study and validate the methods we used. If very

ordered $Cu(dmap)_2$ molecules oriented solely at 120° to each other were observed on the Cu(111) surface, the vdW-DF2 or pure PBE methods could be correct, as shown in **Figure 8**a. In the same manner, more disordered $Cu(dmap)_2$ structures on this Cu surface could indicate that the PBE-D3 or optB88-vdW methods correctly describe $Cu(dmap)_2$ chemisorption in almost any orientation.

Implication for Cu ALD. In a Cu ALD experiment, the substrate was saturated with $Cu(dmap)_2$ when the pulse time exceeded 2.0 s and this gave a growth rate of 0.2 Å/cycle.[11] An indirect ALD experiment with $Cu(dmap)_2$ pulse time longer than 3.0 s afforded a growth rate of 0.50 Å/cycle.[6] In ALD, the precursor molecules should chemisorb strongly on the substrate and react with the co-reagent through surface diffusion. If however the precursor is merely physisorbed on the substrate, reaction of the Cu center with the co-reagent may not be possible because distortion in the structure of physisorbed precursors is very slight and the Cu center is not accessible. The adsorption sites of chemisorbed precursors thus determine the initial position of ALD reactions within the desired monolayer of adsorbates. Regardless of vdW functional, we find that the precursors chemisorb easily with less steric hindrance on rough surfaces such as Cu(332) steps and Cu(643) kinks. Nevertheless, the chemisorption energies on the smooth Cu(111) surface are of the same magnitude (with any given method) and thus, the ALD reactions may take place on both smooth and rough parts of the growing Cu surface simultaneously.

The significant elongation of Cu – N during adsorption indicates that the Cu – N bond breaks in the early stage of ALD reaction cycle as the Cu center gains electrons and is reduced. As a result, the ligands become unstable and the precursor becomes more reactive to the co-reagent. The breaking of the Cu – O bond in the Cu(332)-B configuration of the PBE-D3 calculation illustrates that the Cu – O bond may also break. These indications show that breaking ligand –

Cu bonds is energetically more favourable than the breaking of C – C, C – N, C – O and C – H bonds in the ligand that might lead to C or N impurities, or to deposition of copper oxide. This indicates that the dmap ligand acts as a unit during the ALD of Cu and is an "innocent" ligand that does not participate in the redox reaction. The tendency toward ligand – Cu bond breaking in $Cu(dmap)_2$ may partially explain the success of low temperature ALD of Cu with this molecule. Clean cleavage of the ligand – metal bond is one of the requirements for selecting precursors for ALD of metals.

The Bader charge analysis shows that the Cu atom in the molecule gains 0.2 to 0.4 electrons from the surface on chemisorption, which indicates that the adsorbate Cu atom is partially reduced. We recognise that DFT has systematic errors in the distribution of charge in metal d states. Nevertheless, some reduction of the adsorbate Cu atom should accompany metallic bonding to the surface. This leads to the loss of the precursor's square planar structure and to the linear O – Cu – O motif that attaches to the surface. In order to deposit Cu metal atom from $Cu(dmap)_2$, the adsorbed Cu atom should eventually be reduced to Cu^0 and the ligands should be removed from the surface to pave the way for the next ALD cycle. This is achieved with the reducing agent Et_2Zn in direct ALD[11] and with formic acid and hydrazine in 3-step ALD.[6] Understanding the adsorption of $Cu(dmap)_2$ on the surface provides a base to study the full reaction mechanisms between the reducing agent and the adsorbed precursor, which we will address in our future work.

CONCLUSIONS

In conclusion, we studied the adsorption of the $Cu(dmap)_2$ molecule on different sites on flat and rough Cu surfaces using DFT with various levels of treatment of vdW forces. It is found that the vdW forces are crucial to describe the precursor – substrate interaction. The relative order of

computed adsorption energies for $Cu(dmap)_2$ on Cu surfaces is E_{ads}(PBE-D3) > E_{ads}(optB88-vdW) > E_{ads}(vdW-DF2) > E_{ads}(PBE). We find that the pure PBE and the vdW-DF2 methods yield $Cu(dmap)_2$ chemisorbed selectively at one Cu(111) surface site, while the PBE-D3 method yields chemisorbed structures on Cu(111) at all adsorption sites. The vdW-DF2 functional predicts a chemisorbed structure for three out of four adsorption sites and physisorption for one site, with a relatively large energy for physisorption. For the rough surfaces, all the methods with and without additional vdW forces predict that the molecule chemisorbs on the Cu(332) step and Cu(643) kink.

The breaking of Cu – N or Cu – O bonds as $Cu(dmap)_2$ chemisorbs shows that metal – ligand bonding is broken cleanly during the early stage of Cu ALD, making the molecule reactive to the co-reagent in Cu ALD reactions without unwanted impurities of C, H, O or N. Charge redistribution occurred between the O – Cu – O unit of the molecule and the Cu surface. Bader charge analysis shows that the molecule gains electrons in the chemisorbed structures, with the Cu center in particular being partially reduced.

ASSOCIATED CONTENT

Supporting Information

The calculated geometric parameters of gas-phase $Cu(dmap)_2$. This material is available free of charge via the Internet at http://pubs.acs.org.

AUTHOR INFORMATION

Corresponding Author

*Phone: +353 21 234 6392. E-mail: simon.elliott@tyndall.ie

Notes

The authors declare no competing financial interest.

ACKNOWLEDGEMENTS

We acknowledge support from Science Foundation Ireland (SFI) under the 'ALDesign' Project (grant number 09.IN1.I2628) and from Enterprise Ireland through the Collaborative Centre for Applied Nanotechnology (CCAN) under the ALD300 project. We thank Scott B. Clendenning, Harsono Simka and Roger Nagle from Intel Corporation for fruitful discussions. We acknowledge the SFI and Higher Education Authority funded Irish Centre for High Performance Computing (ICHEC) for access and SFI funded computational resources at the Tyndall National Institute.

REFERENCES

(1) Lim, B. S.; Rahtu, A.; Gordon, R. G. Atomic Layer Deposition of Transition Metals. *Nat. Mater.* **2003**, *2*, 749–754.

(2) Kariniemi, M.; Niinistö, J.; Hatanpää, T.; Kemell, M.; Sajavaara, T.; Ritala, M.; Leskelä, M. Plasma-Enhanced Atomic Layer Deposition of Silver Thin Films. *Chem. Mater.* **2011**, *23*, 2901–2907.

(3) Kwon, J.; Saly, M.; Halls, M. D.; Kanjolia, R. K.; Chabal, Y. J. Substrate Selectivity of (tBu-Allyl)Co(CO)3 during Thermal Atomic Layer Deposition of Cobalt. *Chem. Mater.* **2012**, *24*, 1025–1030.

(4) Mackus, A. J. M.; Garcia-Alonso, D.; Knoops, H. C. M.; Bol, A. A.; Kessels, W. M. M. Room-Temperature Atomic Layer Deposition of Platinum. *Chem. Mater.* **2013**, *25*, 1769–1774.

(5) George, S. M. Atomic Layer Deposition: An Overview. *Chem. Rev.* **2009**, *110*, 111–131.

(6) Knisley, T. J.; Ariyasena, T. C.; Sajavaara, T.; Saly, M. J.; Winter, C. H. Low Temperature Growth of High Purity, Low Resistivity Copper Films by Atomic Layer Deposition. *Chem. Mater.* **2011**, *23*, 4417–4419.

(7) Niskanen, A.; Rahtu, A.; Sajavaara, T.; Arstila, K.; Ritala, M.; Leskelä, M. Radical-Enhanced Atomic Layer Deposition of Metallic Copper Thin Films. *J. Electrochem. Soc.* **2005**, *152*, G25–G28.

(8) Li, Z.; Rahtu, A.; Gordon, R. G. Atomic Layer Deposition of Ultrathin Copper Metal Films from a Liquid Copper(I) Amidinate Precursor. *J. Electrochem. Soc.* **2006**, *153*, C787–C794.

(9) Hagen, D. J.; Connolly, J.; Nagle, R.; Povey, I. M.; Rushworth, S.; Carolan, P.; Ma, P.; Pemble, M. E. Plasma Enhanced Atomic Layer Deposition of Copper: A Comparison of Precursors. *Surf. Coatings Technol.* **2013**, *230*, 3–12.

(10) Hagen, D. J.; Povey, I.; Rushworth, S.; Wrench, J. S.; Keeney, L.; Schmidt, M.; Petkov, N.; Barry, S. T.; Coyle, J. P.; Pemble, M. E. Atomic Layer Deposition of Cu Using a Carbene-Stabilized Cu (I) Silylamide. *J. Mater. Chem. C* **2014**, 9205–9214.

(11) Lee H, B.; Hwang K, J.; Nam, J. W.; Lee U, S.; Kim, J. T.; Koo, S.-M.; Baunemann, A.; Fischer A, R.; Sung M, M. Low-Temperature Atomic Layer Deposition of Copper Metal Thin Films: Self-Limiting Surface Reaction of Copper Dimethylamino-2-Propoxide with Diethylzinc. *Angew. Chemie Int. Ed.* **2009**, *48*, 4536–4539.

(12) Dey, G.; Elliott, S. D. Mechanism for the Atomic Layer Deposition of Copper Using Diethylzinc as the Reducing Agent: A Density Functional Theory Study Using Gas-Phase Molecules as a Model. *J. Phys. Chem. A* **2012**, *116*, 8893–8901.

(13) Kalutarage, L. C.; Clendenning, S. B.; Winter, C. H. Low-Temperature Atomic Layer Deposition of Copper Films Using Borane Dimethylamine as the Reducing Co-Reagent. *Chem. Mater.* **2014**, *26*, 3731–3738.

(14) Ma, Q.; Guo, H.; Gordon, R. G.; Zaera, F. Surface Chemistry of Copper(I) Acetamidinates in Connection with Atomic Layer Deposition (ALD) Processes. *Chem. Mater.* **2011**, *23*, 3325–3334.

(15) Zaera, F. The Surface Chemistry of Thin Film Atomic Layer Deposition (ALD) Processes for Electronic Device Manufacturing. *J. Mater. Chem.* **2008**, *18*, 3521–3526.

(16) Kim, T.; Yao, Y.; Coyle, J. P.; Barry, S. T.; Zaera, F. Thermal Chemistry of Cu(I)-Iminopyrrolidinate and Cu(I)-Guanidinate Atomic Layer Deposition (ALD) Precursors on Ni(110) Single-Crystal Surfaces. *Chem. Mater.* **2013**, *25*, 3630–3639.

(17) Elliott, S. D. Atomic-Scale Simulation of ALD Chemistry. *Semicond. Sci. Technol.* **2012**, *27*, 74008.

(18) Yanagisawa, S.; Lee, K.; Morikawa, Y. First-Principles Theoretical Study of Alq3Al Interfaces: Origin of the Interfacial Dipole. *J. Chem. Phys.* **2008**, *128*, 244704.

(19) Tkatchenko, A.; Romaner, L.; Hofmann, O. T.; Zojer, E.; Ambrosch-Draxl, C.; Scheffler, M. Van Der Waals Interactions Between Organic Adsorbates and at Organic/Inorganic Interfaces. *Mrs Bull.* **2011**, *35*, 435–442.

(20) Kresse, G.; Furthmüller, J. Efficiency of Ab-Initio Total Energy Calculations for Metals and Semiconductors Using a Plane-Wave Basis Set. *Comput. Mater. Sci.* **1996**, *6*, 15–50.

(21) Blochl, P. E. Projector Augmented-Wave Method. *Phys Rev B Condens Matter* **1994**, *50*, 17953–17979.

(22) Perdew, J. P.; Burke, K.; Ernzerhof, M. Generalized Gradient Approximation Made Simple. *Phys. Rev. Lett.* **1996**, *77*, 3865–3868.

(23) Ahlrichs, R.; Bär, M.; Häser, M.; Horn, H.; Kölmel, C. Electronic Structure Calculations on Workstation Computers: The Program System Turbomole. *Chem. Phys. Lett.* **1989**, *162*, 165–169.

(24) Eichkorn, K.; Treutler, O.; Öhm, H.; Häser, M.; Ahlrichs, R. Auxiliary Basis Sets to Approximate Coulomb Potentials. *Chem. Phys. Lett.* **1995**, *240*, 283–290.

(25) Eichkorn, K.; Weigend, F.; Treutler, O.; Ahlrichs, R. Auxiliary Basis Sets for Main Row Atoms and Transition Metals and Their Use to Approximate Coulomb Potentials. *Theor. Chem. Acc.* **1997**, *97*, 119–124.

(26) Weigend, F.; Ahlrichs, R. Balanced Basis Sets of Split Valence, Triple Zeta Valence and Quadruple Zeta Valence Quality for H to Rn: Design and Assessment of Accuracy. *Phys. Chem. Chem. Phys.* **2005**, *7*, 3297–3305.

(27) Henkelman, G.; Uberuaga, B. P.; Jonsson, H. A Climbing Image Nudged Elastic Band Method for Finding Saddle Points and Minimum Energy Paths. *J. Chem. Phys.* **2000**, *113*, 9901–9904.

(28) Henkelman, G.; Jónsson, H. Improved Tangent Estimate in the Nudged Elastic Band Method for Finding Minimum Energy Paths and Saddle Points. *J. Chem. Phys.* **2000**, *113*, 9978.

(29) Liu, W.; Tkatchenko, A.; Scheffler, M. Modeling Adsorption and Reactions of Organic Molecules at Metal Surfaces. *Acc. Chem. Res.* **2014**, *47*, 3369–3377.

(30) Liu, W.; Ruiz, V. G.; Zhang, G.-X.; Santra, B.; Ren, X.; Scheffler, M.; Tkatchenko, A. Structure and Energetics of Benzene Adsorbed on Transition-Metal Surfaces: Density-Functional Theory with van Der Waals Interactions Including Collective Substrate Response. *New J. Phys.* **2013**, *15*, 053046.

(31) Yildirim, H.; Greber, T.; Kara, A. Trends in Adsorption Characteristics of Benzene on Transition Metal Surfaces: Role of Surface Chemistry and van Der Waals Interactions. *J. Phys. Chem. C* **2013**, *117*, 20572–20583.

(32) Toyoda, K.; Nakano, Y.; Hamada, I.; Lee, K.; Yanagisawa, S.; Morikawa, Y. First-Principles Study of Benzene on Noble Metal Surfaces: Adsorption States and Vacuum Level Shifts. *Surf. Sci.* **2009**, *603*, 2912–2922.

(33) Liu, W.; Carrasco, J.; Santra, B.; Michaelides, A.; Scheffler, M.; Tkatchenko, A. Benzene Adsorbed on Metals: Concerted Effect of Covalency and van Der Waals Bonding. *Phys. Rev. B* **2012**, *86*, 245405.

(34) Carrasco, J.; Liu, W.; Michaelides, A.; Tkatchenko, A. Insight into the Description of van Der Waals Forces for Benzene Adsorption on Transition Metal (111) Surfaces. *J. Chem. Phys.* **2014**, *140*, 084704.

(35) Rosa, M.; Corni, S.; Di Felice, R. Van Der Waals Effects at Molecule-Metal Interfaces. *Phys. Rev. B* **2014**, *90*, 125448.

(36) Grimme, S. Semiempirical GGA-Type Density Functional Constructed with a Long-Range Dispersion Correction. *J. Comput. Chem.* **2006**, *27*, 1787–1799.

(37) Grimme, S.; Antony, J.; Ehrlich, S.; Krieg, H. A Consistent and Accurate Ab Initio Parametrization of Density Functional Dispersion Correction (DFT-D) for the 94 Elements H-Pu. *J. Chem. Phys.* **2010**, *132*, 154104–154119.

(38) Tonigold, K.; Gross, A. Adsorption of Small Aromatic Molecules on the (111) Surfaces of Noble Metals: A Density Functional Theory Study with Semiempirical Corrections for Dispersion Effects. *J. Chem. Phys.* **2010**, *132*, 224701.

(39) Baran, J. D.; Larsson, J. A. Theoretical Insights into Adsorption of Cobalt Phthalocyanine on Ag(111): A Combination of Chemical and van Der Waals Bonding. *J. Phys. Chem. C* **2013**, *117*, 23887–23898.

(40) Baran, J. D.; Larsson, J. A. Structure and Energetics of Shuttlecock-Shaped Tin-Phthalocyanine on Ag(111): A Density Functional Study Employing Dispersion Correction. *J. Phys. Chem. C* **2012**, *116*, 9487–9497.

(41) Grimme, S.; Ehrlich, S.; Goerigk, L. Effect of the Damping Function in Dispersion Corrected Density Functional Theory. *J. Comput. Chem.* **2011**, *32*, 1456–1465.

(42) Dion, M.; Rydberg, H.; Schroder, E.; Langreth, D. C.; Lundqvist, B. I. Van Der Waals Density Functional for General Geometries. *Phys. Rev. Lett.* **2004**, *92*, 246401.

(43) Jiří, K.; David, R. B.; Angelos, M. Chemical Accuracy for the van Der Waals Density Functional. *J. Phys. Condens. Matter* **2010**, *22*, 22201.

(44) Ziambaras, E.; Kleis, J.; Schröder, E.; Hyldgaard, P. Potassium Intercalation in Graphite: A van Der Waals Density-Functional Study. *Phys. Rev. B* **2007**, *76*, 155425.

(45) Hamada, I. A van Der Waals Density Functional Study of Ice Ih. *J. Chem. Phys.* **2010**, *133*, 214503.

(46) Puzder, A.; Dion, M.; Langreth, D. C. Binding Energies in Benzene Dimers: Nonlocal Density Functional Calculations. *J. Chem. Phys.* **2006**, *124*, 164105.

(47) Tkatchenko, A.; Scheffler, M. Accurate Molecular Van Der Waals Interactions from Ground-State Electron Density and Free-Atom Reference Data. *Phys. Rev. Lett.* **2009**, *102*, 73005.

(48) Ruiz, V. G.; Liu, W.; Zojer, E.; Scheffler, M.; Tkatchenko, A. Density-Functional Theory with Screened van Der Waals Interactions for the Modeling of Hybrid Inorganic-Organic Systems. *Phys. Rev. Lett.* **2012**, *108*, 146103.

(49) Lide, D. CRC Handbook of Chemistry and Physics: A Ready-Reference Book of Chemical and Physical Data. Ed. 82 (2001-2002). **2004**, 2610.

(50) Henkelman, G.; Arnaldsson, A.; Jónsson, H. A Fast and Robust Algorithm for Bader Decomposition of Charge Density. *Comput. Mater. Sci.* **2006**, *36*, 354–360.

(51) Vanpoucke, D. E. P.; Brocks, G. Formation of Pt-Induced Ge Atomic Nanowires on Pt/Ge(001): A Density Functional Theory Study. *Phys. Rev. B* **2008**, *77*, 241308.

(52) Tersoff, J.; Hamann, D. R. Theory of the Scanning Tunneling Microscope. *Phys. Rev. B* **1985**, *31*, 805–813.

(53) Becker, R.; Devi, A.; Weiß, J.; Weckenmann, U.; Winter, M.; Kiener, C.; Becker, H. W.; Fischer, R. A. A Study on the Metal Organic CVD of Pure Copper Films from Low Cost Copper(II) Dialkylamino-2-Propoxides: Tuning the Thermal Properties of the Precursor by Small Variations of the Ligand. *Chem. Vap. Depos.* **2003**, *9*, 149–156.

(54) Maimaiti, Y.; Nolan, M.; Elliott, S. D. Reduction Mechanisms of the CuO(111) Surface through Surface Oxygen Vacancy Formation and Hydrogen Adsorption. *Phys. Chem. Chem. Phys.* **2014**, 3036–3046.

(55) Franke, J.-H.; Kosov, D. S. Adsorption of Lactic Acid on Chiral Pt Surfaces--a Density Functional Theory Study. *J. Chem. Phys.* **2013**, *138*, 084705.

(56) Vollmer, S.; Birkner, A.; Lukas, S.; Witte, G.; Wöll, C. Nanopatterning of Copper (111) Vicinal Surfaces by Oxygen-Induced Mesoscopic Faceting. *Appl. Phys. Lett.* **2000**, *76*, 2686–2688.

(57) Baber, A. E.; Gellman, A. J.; Sholl, D. S.; Sykes, E. C. H. The Real Structure of Naturally Chiral Cu{643}. *J. Phys. Chem. C* **2008**, *112*, 11086–11089.

(58) Mercurio, G.; McNellis, E. R.; Martin, I.; Hagen, S.; Leyssner, F.; Soubatch, S.; Meyer, J.; Wolf, M.; Tegeder, P.; Tautz, F. S.; et al. Structure and Energetics of Azobenzene on Ag(111): Benchmarking Semiempirical Dispersion Correction Approaches. *Phys. Rev. Lett.* **2010**, *104*, 036102.